

Sign reversal of magnetoresistance in a perovskite nickelate by electron dopingKoushik Ramadoss,^{1,*} Nirajan Mandal,^{2,3} Xia Dai,⁴ Zhong Wan,² You Zhou,⁵ Leonid Rokhinson,^{2,3,6} Yong P. Chen,^{2,3,6} Jiangpin Hu,² and Shriram Ramanathan¹¹*School of Materials Engineering, Purdue University, West Lafayette, Indiana 47907, USA*²*Department of Physics and Astronomy, Purdue University, West Lafayette, Indiana 47907, USA*³*Birck Nanotechnology Center, Purdue University, West Lafayette, Indiana 47907, USA*⁴*Institute of Physics, Chinese Academy of Sciences, P.O. Box 603, Beijing 100190, China*⁵*School of Engineering and Applied Sciences, Harvard University, Cambridge, Massachusetts 02138, USA*⁶*School of Electrical and Computer Engineering, Purdue University, West Lafayette, Indiana 47907, USA*

(Received 31 July 2016; revised manuscript received 14 November 2016; published 9 December 2016)

We present low temperature resistivity and magnetotransport measurements conducted on pristine and electron doped SmNiO_3 (SNO). The low temperature transport in both pristine and electron-doped SNO shows a Mott variable range hopping with a substantial decrease in localization length of carriers by one order in the case of doped samples. Undoped SNO films show a negative magnetoresistance (MR) at all temperatures characterized by spin fluctuations with the evolution of a positive cusp at low temperatures. In striking contrast, upon electron doping of the films via hydrogenation, we observe a crossover to a linear nonsaturating positive MR $\sim 0.2\%$ at 50 K. The results signify the role of localization phenomena in tuning the magnetotransport response in doped nickelates. Ionic doping is therefore a promising approach to tune magnetotransport in correlated perovskites.

DOI: [10.1103/PhysRevB.94.235124](https://doi.org/10.1103/PhysRevB.94.235124)**I. INTRODUCTION**

Rare-earth nickelates (RNiO_3) display a rich phase diagram including a metal-insulator transition and antiferromagnetic transition that are controlled by the radius of the rare-earth ion (R^{3+}). The metal-insulator transition temperature decreases with an increase in radii of the rare-earth ion [1–3]. The transition to the antiferromagnetic state (T_N) occurs at the same temperature as the metal-insulator transition (T_{MI}) for the lighter rare-earth ($R = \text{Nd, Pr}$), whereas for heavier elements, $T_N < T_{MI}$ with T_N progressively decreasing from Sm to Lu. An essential feature of the magnetic transition is that it is first order in nature when $T_N = T_{MI}$, whereas nickelates with $T_N < T_{MI}$ exhibit a second-order magnetic transition.

One of the remarkable features of these nickelate systems is that they can be tuned across a variety of phases like strange metals with non-Fermi liquid behavior, paramagnetic insulator and antiferromagnetic insulator by means of strain, heterostructuring and doping resulting in novel effects like quenching of antiferromagnetic phase in strained NdNiO_3 [4], metal-insulator transition in ultrathin films of LaNiO_3 [5,6], suppression of paramagnetic insulating phase [7], spin density wave order in nickelate superlattices [8,9], and band gap modulation in SmNiO_3 [10]. Carrier doping by electrostatic gating or chemical substitution is an active field to modify electronic properties of nickelates [11–15] and at the same time serving as a tool to understand and possibly control the metal-insulator transition (MIT) phenomenon in nickelates. Earlier studies regarded nickelates as charge transfer insulators [16], whereas in recent works, the origin of insulating phase in nickelates has been attributed to charge disproportionation of the Ni site with an accompanying structural change from orthorhombic to monoclinic phase [17–20]. Electrolytic gating measurements on thin films of NdNiO_3 point towards a

Mott-type mechanism where the MIT is driven by a critical carrier density that is controlled by the gate voltage [11]. Electrostatic gating and hole doping by Sr have been used to tune T_{MI} in NdNiO_3 [12,21]. Nickelates when substituted with a ferromagnetic element like Co have been shown to exhibit spin-glass behavior due to competing ferromagnetic and antiferromagnetic interactions [22]. Chemical doping by hydrogen incorporation into nickelate lattices has been shown to modify the ground state properties by inducing a colossal change in the resistivity that can be reversed by removing the dopant species from the lattice [10]. Nickelates have also been proposed to serve as candidate systems for understanding high temperature superconductivity due to the rich physics inherent in d -orbital nondegeneracy [23–25]. These interesting observations open up a possibility of realizing new electrical and magnetic ground states for the electron-doped nickelates.

Previous experiments on pristine nickelates have shown the low temperature transport to be dominated by a hopping mechanism. In the case of NdNiO_3 , the low temperature resistivity behavior was modeled as a combination of activation and variable range hopping (VRH) [26]. SNO thin films have also been shown to exhibit variable range hopping at low temperatures [27]. These results signify the presence of localized states that dominate the low-temperature phase of nickelates. Unlike conventional semiconductors, nickelates display a nonmonotonic behavior in magnetoresistance which has been attributed to its antiferromagnetic nature [28,29]. Nonmonotonic behavior in magnetoresistance has also been seen in other correlated oxide systems of SrTiO_3 quantum wells sandwiched between SmTiO_3 , and the results were interpreted in terms of spin scattering of carriers [30]. Recently the influence of strong localization and disorder on the ground state properties of topological insulator thin films were studied using magnetotransport which showed a reversal in the sign of magnetoresistance (MR) [31].

In this paper, we present a method to tune the magnetotransport properties of perovskite nickelates by electron doping

*koushik@purdue.edu, shriram@purdue.edu

via hydrogenation. Electron occupancy in the Ni orbitals is modified and simultaneously disorder is introduced due to the interstitial dopants. This creates a rich environment to tune magnetic order and we model the results taking into account the spins in localized states.

II. EXPERIMENTS

SmNiO₃ (SNO) thin films (100 nm) were prepared by cosputtering from Sm and Ni targets in Ar/O₂ atmosphere onto a single crystal lanthanum aluminate substrate [33]. Metal contacts [Pt/Ti/Au (100/5/100 nm)] were then patterned on the films for four-probe electrical transport measurements. Doping of these films was carried out by annealing them at 200 °C in forming gas (5% H₂ in N₂) for 3 h. During this process Pt electrodes serve as a catalyst to dissociate the H₂ into atomic hydrogen which then splits into H⁺ and e⁻ which are subsequently incorporated into the SNO lattice thereby changing the valence state of nickel to Ni²⁺ [10]. Dopants are incorporated robustly into the material via the anneal process. We refer to the electron-doped SNO as HSNO henceforth in the paper. The transport measurements were carried out in a Quantum Design Dynacool physical properties measurement system (PPMS) system in a temperature range of 2.2–300 K and magnetic field up to 9 T with a small signal ac excitation of 10 nA. The measurements of HSNO could be made only down to about 40 K as the resistivity of these films increased beyond the measurable range of the PPMS system in a four wire configuration. Conducting atomic force microscopy (CAFM) measurements were performed at room temperature using an Asylum MFP3D stand-alone atomic force microscope and Asylum ASYLEC-01 conductive tips (Si coated with Ti/Ir). The bias (1 V_{DC}) was applied to the sample with a 1 MΩ resistor in series while the AFM tip is grounded. The resistor serves to limit the maximum current so as to avoid any damage to the metal coating on the tip. The current flowing from the sample to the tip is amplified using current amplifiers (dual gain ORCA) with a sensitivity of 1 V/nA and 1 V/μA. The scan area was chosen to be 5 × 5 μm² with a scan rate of 1 Hz. Raman spectra were recorded using a confocal microscope system with an excitation laser of 532 nm. The laser spot size is ~1 μm² enabling us to scan across the SNO/HSNO boundary. Raman modes were also calculated from first principles and the details are presented in the Supplemental Material [32].

III. RESULTS AND DISCUSSION

The resistivity of pristine SNO and HSNO films displays an insulating behavior over the entire temperature range of our measurements. Rare-earth nickelates are found to exhibit variable range hopping at low temperatures [26,34] where it is energetically favorable for an electron to hop to a site that is closer in energy than the nearest neighbor leading to VRH and is given by

$$\rho(T) = \rho_1 \exp\left(\frac{T_0}{T}\right)^p, \quad (1)$$

where ρ_1 is the prefactor, T_0 is the characteristic temperature, and p is the exponent dependent on the conduction mechanism. The type of VRH conduction is dependent on the details

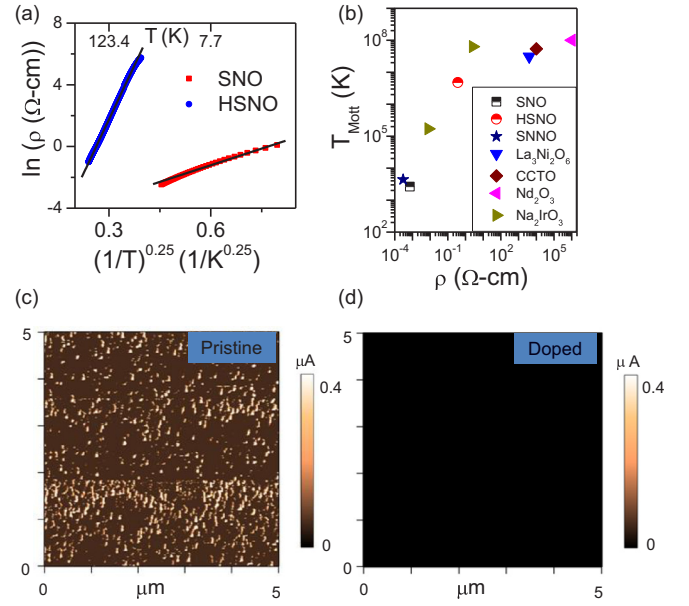


FIG. 1. (a) Plot of $\ln(\rho)$ vs $T^{-1/4}$ for SNO and HSNO. Black lines are linear fits indicating Mott VRH. (b) Comparison of T_M vs ρ for SNO and HSNO films with other oxide systems: SNO, HSNO (this work), Sm_{0.5}Nd_{0.5}NiO₃ (SNNNO) [34], La₃Ni₂O₆ [35], CaCu₃Ti₄O₁₂ (CCTO) [36], Nd₂O₃ [37], Na₂IrO₃ [38]. (c), (d) CAFM images for SNO and HSNO over a region of 5 × 5 μm². CAFM of the doped sample appears dark due to large suppression of electronic conductivity.

of the density of states (DOS) around Fermi energy (E_F). It was shown by Mott [39] that for a constant DOS, $p = 1/(D + 1)$ where D is the dimensionality of the system. In three dimensions, $p = 1/4$ and T_0 is given by [40,41]

$$T_0 \equiv T_{\text{Mott}} = \frac{18}{k_B N(E_F) \xi^3}, \quad (2)$$

where $N(E_F)$ is the DOS near E_F and ξ is the localization length. When Coulomb interaction between charge carriers is taken into account, a gap appears in the DOS near E_F and one can show that $p = 1/2$. This mechanism is known as Efros-Shklovskii VRH [42] where $T_0 = \frac{2.8 e^2}{4\pi\epsilon k_B \xi}$, ϵ being the dielectric permittivity.

In our experiments, pristine SNO film displays a Mott VRH mechanism at low temperature ($T < 20$ K) as evident from the linearity of $\ln(\rho)$ vs $T^{-0.25}$ [Fig. 1(a)]. The HSNO film shows remarkably strong localization behavior with Mott VRH over a larger temperature range from 300 to 40 K. The linear fits yield $T_{\text{Mott}} = 2.6 \times 10^3$ K for SNO and using Eq. (2), we find $\xi \sim 37$ nm taking $N(E_F) = 1.5 \times 10^{18}$ eV⁻¹ cm⁻³. For HSNO, the magnitude of T_{Mott} ($T_{\text{Mott}} = 4.7 \times 10^6$ K) is about three orders of magnitude higher than that of SNO with a relatively small $\xi \sim 3$ nm. Here we have assumed $N(E_F)$ to remain approximately the same even after doping. The reason is that unlike other oxide semiconductors [43,44] where hydrogen doping introduces states near conduction band, in SNO, hydrogen doping leads to a large change in band gap of the material [10]. To check the consistency of the fits for the Mott VRH in SNO and HSNO, we have calculated the hopping distance $R_h = \left(\frac{9\xi}{8\pi k_B T N(E_F)}\right)^{1/4}$ and the average hopping energy

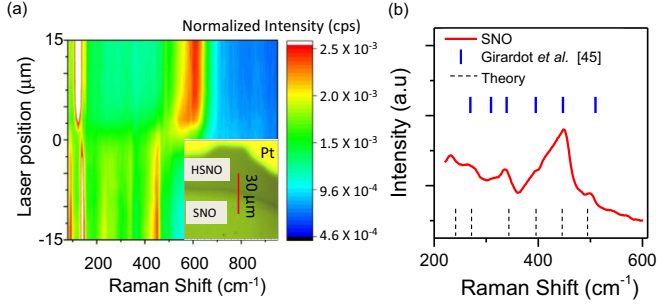


FIG. 2. (a) Raman scan taken at various positions along the red line across the SNO/HSNO interface (shown in the inset). The inset shows the optical image of the electrode (Pt), SNO and HSNO regions. (b) Raman spectrum of pristine SNO (red) being compared with experimental data (blue line) from literature (Girardot *et al.* [45]). The vertical dotted lines (black) correspond to those predicted by theory.

$W_h = \frac{3}{4\pi R^3 N(E_F)}$. We find that for both pristine and doped SNO films, the conditions $\frac{R_h}{\xi} > 1$ and $\frac{W_h}{k_B T} > 1$ are satisfied for the validity of the Mott VRH process. A comparison of T_{Mott} for SNO and HSNO with various systems of correlated oxides is shown in Fig. 1(b). We find good agreement for SNO with other nickelates [34] and HSNO falls into the category of oxides showing a stronger carrier localization with higher T_{Mott} . These correlated oxides also show a trend with an increase in T_{Mott} as ρ of the film increases signifying that highly resistive films display a stronger localization behavior. We have also carried out transport at nanoscale using CAFM which measures the current spatially across the sample. The CAFM images of both pristine and electron-doped SNO grown on Si/SiO₂ substrate are shown in Figs. 1(c) and 1(d). The current level in SNO is about four orders of magnitude larger than that of HSNO. The current profile of HSNO is homogeneous indicating the spatial homogeneity of doping.

To further understand the effects of electron doping on the phonon modes in nickelates, we have performed spatial Raman mapping of the SNO-HSNO region which is shown in Fig. 2(a). The optical image of the sample near the platinum electrode is shown in the inset of Fig. 2(a) where we see a clear optical contrast between the SNO and HSNO regions and the line (length 30 μm) over which the Raman scan was performed is shown as red. As shown in the Raman scan, a clear distinction is seen in the Raman modes of the SNO and HSNO regions. The mode with larger intensity at $\sim 450 \text{ cm}^{-1}$ corresponding to the A_g mode seen in the SNO films is clearly absent in HSNO where a new mode emerges at 617 cm^{-1} . The emergence of a new mode in HSNO is possibly due to breaking of some underlying symmetry in the nickelate lattice. The uniformity of the Raman scan is also indicative of the spatial homogeneity of the SNO and HSNO regions. Perovskite nickelates in their insulating state exhibit monoclinic distortion ($P2_1/n$ space group) with 24 Raman-active modes which are represented as [8,45]

$$\Gamma_{\text{Raman}} = 12A_g + 12B_g. \quad (3)$$

Using DFT calculations (details in the Supplemental Material) we have determined all 24 modes for pristine SNO

TABLE I. Comparison of Raman frequencies (in units of cm^{-1}) of SNO observed experimentally to those from DFT calculations.

Experiment	92.2	141.3	230.4	269.5	386.2	428.4	450.9	499.1
DFT	94.9	139.4	237.5	266.7	393.3	429.7	444.9	494.6
Mode	A_g	A_g	B_g	B_g	A_g	B_g	A_g	B_g

and a comparison with experimentally observed modes is shown in Table I. We obtain good agreement between theory and experiment with rms error $\sim 5 \text{ cm}^{-1}$. Our calculations show that the mode at 444.9 cm^{-1} is mainly contributed from the movements of O atoms in the $8d$ Wyckoff positions. In Fig. 2(b), we show the Raman spectrum in pristine SNO which is in good agreement with that reported in Ref. [45]. The dotted lines correspond to modes predicted by density functional theory (DFT).

We then investigate the mechanism of strong carrier localization in doped nickelates by measuring the magnetoresistance ($\text{MR} = \{[\rho(H) - \rho(0)]/\rho(0)\}$) in both SNO and HSNO films at various temperatures. In SNO, MR which is positive at low fields ($H \lesssim 3 \text{ T}$) shows a crossover to negative magnetoresistance behavior at higher fields [Fig. 3(a)]. The positive MR is suppressed at higher temperatures ($T \gtrsim 10 \text{ K}$). The field (H_m) at which crossover in MR occurs exhibits a nonmonotonic response as a function of temperature with a minima at 5 K [Fig. 3(d)]. The positive MR seen at low fields is about 0.7% at 2.24 K and decreases with an increase in temperature. The magnitude of negative MR (taken at 9 T) reaches its maximum value of $\sim 2.5\%$ at 5 K and displays

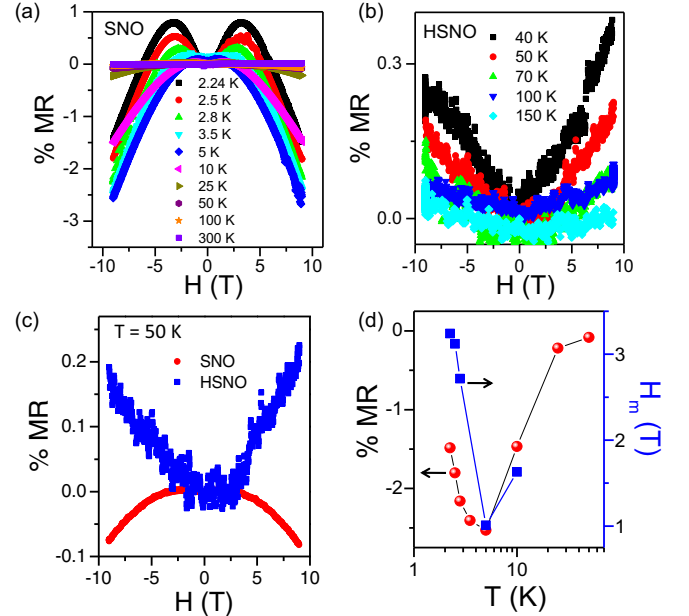


FIG. 3. (a) Magnetoresistance (in percent) vs H for SNO film at various temperatures. (b) Magnetoresistance (in percent) vs H for HSNO film at various temperatures. (c) Comparison of magnetoresistance (in percent) vs H for SNO and HSNO film at $T = 50 \text{ K}$. (d) Magnetoresistance (in percent) (left y axis) vs T at $H = 9 \text{ T}$ for SNO film. Crossover field H_m (right y axis) vs T for SNO film.

a similar trend to that of H_m [Fig. 3(d)]. For $T > 5$ K, the negative MR decreases in magnitude and is eventually suppressed by ~ 100 K. A remarkably different behavior is seen in HSNO films where the MR is positive over the entire field range and its value decreases as temperature is increased [Fig. 3(b)]. The MR for pristine and electron-doped film at $T = 50$ K is shown in Fig. 3(c) for comparison. A clear sign reversal from negative to positive magnetoresistance is seen with electron doping. In systems of correlated iridates, sign reversal in MR has been observed as a function of temperature [46]. We emphasize that the sign reversal in MR is caused by the incorporation of dopants and rule out any effects of temperature (details in the Supplemental Material).

In order to understand the connection between the magnetoresistance behavior and strong carrier localization, we look at the different mechanisms that contribute to magnetoresistance in correlated oxides. Negative MR can arise from various mechanisms such as weak localization, hopping conduction, and magnetic scattering, while mechanisms such as wave function shrinkage and strong spin orbit scattering lead to positive MR. After a systematic analysis (detailed in the Supplemental Material) of the data using various models for MR, the MR behavior in pristine SNO films can be modeled by two competing mechanisms resulting from correlation among spins in localized states. Frydman *et al.* [47,48] had proposed that in samples exhibiting variable range hopping conduction, exchange correlation among spins in different hopping sites can give rise to positive MR (negative magnetoconductance) that tends to saturate at a characteristic field called spin alignment fields. According to this model, the magnetoconductance (MC = $\frac{\Delta\sigma}{\sigma} = \{\sigma(H) - \sigma(0)\}/\sigma(0)$) is given by

$$\frac{\Delta\sigma}{\sigma} = -A_e \frac{H^2}{H^2 + H_e^2}, \quad (4)$$

where A_e is the saturation value, $H_e = a \frac{k_B T}{\mu_B} \left(\frac{T_{\text{Mott}}}{T}\right)^{0.25}$ is the spin alignment field, a is a constant of the order unity, and μ_B is the Bohr magneton. The negative MR at larger fields can be modeled by hopping conduction through the Zeeman effect [49,50]. According to this model, the applied field shifts the Fermi level E_F by the Zeeman energy ($g\mu_B H$) and causes splitting of the spin-up and spin-down subbands and redistributes carriers among the localized states. This leads to delocalization of the carriers thereby leading to a decrease in resistance. The MC according to this model is given as

$$\frac{\Delta\sigma}{\sigma} = c \left(\frac{g\mu_B H}{E_c - E_F} \right)^2 \left(\frac{T_{\text{Mott}}}{T} \right)^{0.5}, \quad (5)$$

where g is the Landé g factor, E_c is the mobility edge, and c is a constant of the order of unity. Combining the above two models, MC in SNO is expressed as

$$\frac{\Delta\sigma}{\sigma} = -A_e \frac{H^2}{H^2 + H_e^2} + c \left(\frac{g\mu_B H}{E_c - E_F} \right)^2 \left(\frac{T_{\text{Mott}}}{T} \right)^{0.5}. \quad (6)$$

Figure 4(a) shows the fits for MC for SNO at different temperatures. Here we take $(E_c - E_F) \sim 0.1$ eV, typical band gap in SNO [51] and the error bars obtained for the fit parameters are within 5%. The model is valid for $\left(\frac{T_{\text{Mott}}}{T}\right)^{0.25} \gg 1$ which is true in our case. Figure 4(b) shows H_e obtained from the fit agree well with the theoretical prediction for

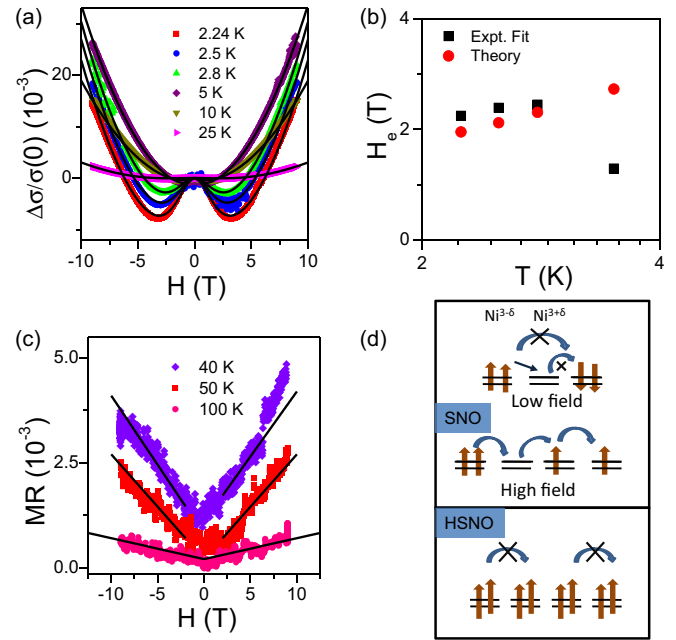


FIG. 4. (a) Magnetoconductance vs H for SNO film at various temperatures. Solid black lines are fits according to Eq. (6). (b) Temperature dependence of fit parameter H_e (black squares). Red squares indicate theoretical predictions for H_e . (c) Magnetoresistance vs H for HSNO film at various temperatures. Solid black lines are a guide to the eye. (d) Illustration of mechanisms leading to magnetoresistance in SNO (top panel) and HSNO (bottom panel) films.

$T < 5$ K. We also observe reasonable agreement of the fit parameter c with the model which predicts $c \sim 1$. Figure 4(d) (top panel) shows a simplified schematic representation of the magnetotransport in pristine SNO samples at low temperatures which can be understood from a framework of interacting spins localized at different sites [28–30,52]. Assuming charge disproportionation, the nickelate lattice can be modeled as $S = 1$ sites antiferromagnetically coupled via $S = 0$ sites [20]. Although it is well known that rare-earth nickelates exhibit antiferromagnetic order at low temperatures, the precise magnetic structure is complex with proposals of collinear and noncollinear magnetic structures from neutron [53] and soft x-ray scattering studies [18] and a canted antiferromagnetic state from magnetic susceptibility measurements [54]. Our measurements at low temperatures ($T \lesssim 5$ K) yield a positive cusp in the MR signifying the presence of interacting spins that are frozen as seen in systems exhibiting a spin-glass phase [55,56]. An application of finite field (~ 3.5 T) destroys the frozen spin state leading to enhancement in spin scattering resulting in negative MR. At such large fields, the spins are polarized enhancing spin fluctuations and hopping rate of carriers resulting in a decrease in resistance with an increase in field. At higher temperatures ($T > 10$ K), larger thermal energy suppresses the positive cusp, resulting only in negative MR that is quadratic in field. Signatures of such a low-temperature spin-glass-like state have been seen in MR and magnetization measurements in other correlated oxides such as iridates [55]. The field scale of ~ 3.5 T obtained in our experiments is consistent with the hopping energy in the VRH

regime which is ~ 0.5 meV, thus signifying the role of spin correlations that govern the low-temperature transport.

The electron-doped sample shows a remarkably distinct signature in magnetotransport with a linear positive magnetoresistance as against pristine films that exhibit negative magnetoresistance [Fig. 4(c)]. Tuning the MR in oxides can be achieved by the introduction of dopants or defects. Incorporation of Mn dopants in ZnO changes the intrinsic positive MR (due to wave function squeezing) to a giant negative MR arising from spin scattering caused by Mn moments [57]. Ferromagnetism is seen in hydrogen-doped ZnO single crystals investigated by magnetotransport [58]. Nonmonotonous magnetoresistance observed in proton implanted Li-doped ZnO wires has been attributed to enhancement of spin polarization due to doping [59]. Positive magnetoresistance is commonly observed in systems in a strongly localized regime with VRH conduction. In such systems, the wave function of the localized charge carrier shrinks under the application of a magnetic field thereby leading to a positive MR [42,60]. Such models predict an exponential dependence of MR on the magnetic field. But we do not see such a behavior in our thin films. In experiments on strongly correlated oxides, linear positive MR has also been seen in SrTiO₃ crystals and was attributed to the presence of point defects [61]. Nonsaturating linear MR has also been observed in high mobility semiconductors due to the fluctuations in the mobility of the carriers [62,63] and semiconductors in a strongly localized regime [64]. However, to qualitatively understand the mechanism in HSNO, we need to look into the details of the doping in SNO films. When SNO is annealed in the hydrogen environment, the hydrogen splits into a proton and an electron at the platinum electrode-SNO interface. The electron goes into the e_g orbital of transition metal changing its valence state to Ni²⁺. From Hund's rule, the two electrons in the e_g orbital are likely to have the same

spin resulting in a high spin state ($S = 1$) which is a strongly correlated state [shown in the bottom panel of Fig. 4(d)]. In such a case, one can expect a large fraction of Ni²⁺ leading to strong correlation among localized sites along with significant disorder from the protons in the lattice. The linear positive MR in the electron-doped nickelates might therefore result from a combination of disorder, localization, and strong correlations. Such a scenario is seen in systems of organic semiconductor V(TCNE)₂ exhibiting localization and magnetic order. In such systems, it has been shown that exchange interactions between spins of V²⁺ and the upper π^* subband of TCNE lead to linear MR [65,66]. Thus electron-doped nickelates presents itself as a system with tunable magnetotransport mediated by ionic doping and could be of potential interest in the growing field of magneto-ionic devices [67].

IV. SUMMARY

To summarize, we have shown that it is possible to tune the sign of magnetoresistance in perovskite nickelates via electron doping. Charge localization through orbital occupancy control is therefore an effective route to also modulate magnetotransport in these materials. Further experimental probes such as resonant x-ray scattering and neutron diffraction would be valuable to reveal the underlying magnetic structure in electron-doped nickelates.

ACKNOWLEDGMENTS

The authors acknowledge financial support from ARO W911NF-16-1-0289 and AFOSR FA9550-15-1-0219. This work was performed in part at the Birck Center for Nanotechnology, Purdue University.

-
- [1] G. Catalan, *Phase Transitions* **81**, 729 (2008).
- [2] J.-S. Zhou, J. B. Goodenough, and B. Dabrowski, *Phys. Rev. Lett.* **95**, 127204 (2005).
- [3] S. Middey, J. Chakhalian, P. Mahadevan, J. W. Freeland, A. J. Millis, and D. D. Sarma, *Annu. Rev. Mater. Res.* **46**, 305 (2016).
- [4] J. Liu, M. Kargarian, M. Kareev, B. Gray, P. J. Ryan, A. Cruz, N. Tahir, Y.-D. Chuang, J. Guo, J. M. Rondinelli *et al.*, *Nat. Commun.* **4**, 2714 (2013).
- [5] R. Scherwitzl, S. Gariglio, M. Gabay, P. Zubko, M. Gibert, and J.-M. Triscone, *Phys. Rev. Lett.* **106**, 246403 (2011).
- [6] A. Boris, Y. Matiks, E. Benckiser, A. Frano, P. Popovich, V. Hinkov, P. Wochner, M. Castro-Colin, E. Detemple, V. K. Malik *et al.*, *Science* **332**, 937 (2011).
- [7] S. Catalano, M. Gibert, V. Bisogni, O. Peil, F. He, R. Sutarto, M. Viret, P. Zubko, R. Scherwitzl, A. Georges *et al.*, *APL Mater.* **2**, 116110 (2014).
- [8] M. Hepting, M. Minola, A. Frano, G. Cristiani, G. Logvenov, E. Schierle, M. Wu, M. Bluschke, E. Weschke, H.-U. Habermeier *et al.*, *Phys. Rev. Lett.* **113**, 227206 (2014).
- [9] G. Berner, M. Sing, F. Pfaff, E. Benckiser, M. Wu, G. Cristiani, G. Logvenov, H.-U. Habermeier, M. Kobayashi, V. N. Strocov *et al.*, *Phys. Rev. B* **92**, 125130 (2015).
- [10] J. Shi, Y. Zhou, and S. Ramanathan, *Nat. Commun.* **5**, 4860 (2014).
- [11] R. Scherwitzl, P. Zubko, I. G. Lezama, S. Ono, A. F. Morpurgo, G. Catalan, and J.-M. Triscone, *Adv. Mater.* **22**, 5517 (2010).
- [12] J. Son, B. Jalan, A. P. Kajdos, L. Balents, S. J. Allen, and S. Stemmer, *Appl. Phys. Lett.* **99**, 192107 (2011).
- [13] J. Shi, S. D. Ha, Y. Zhou, F. Schoofs, and S. Ramanathan, *Nat. Commun.* **4**, 2676 (2013).
- [14] J. Ngai, F. Walker, and C. Ahn, *Annu. Rev. Mater. Res.* **44**, 1 (2014).
- [15] S. Babel, A. J. Hauser, A. M. Glauddell, T. E. Mates, S. Stemmer, and M. L. Chabiny, *Appl. Phys. Lett.* **106**, 122102 (2015).
- [16] J. B. Torrance, P. Lacorre, A. I. Nazzal, E. J. Ansaldo, and C. Niedermayer, *Phys. Rev. B* **45**, 8209 (1992).
- [17] U. Staub, G. I. Meijer, F. Fauth, R. Allenspach, J. G. Bednorz, J. Karpinski, S. M. Kazakov, L. Paolasini, and F. d'Acapito, *Phys. Rev. Lett.* **88**, 126402 (2002).
- [18] V. Scagnoli, U. Staub, A. M. Mulders, M. Janousch, G. I. Meijer, G. Hammerl, J. M. Tonnerre, and N. Stojic, *Phys. Rev. B* **73**, 100409 (2006).

- [19] M. Medarde, C. Dallera, M. Grioni, B. Delley, F. Vernay, J. Mesot, M. Sikora, J. A. Alonso, and M. J. Martínez-Lope, *Phys. Rev. B* **80**, 245105 (2009).
- [20] S. Johnston, A. Mukherjee, I. Elfimov, M. Berciu, and G. A. Sawatzky, *Phys. Rev. Lett.* **112**, 106404 (2014).
- [21] J. Alonso, M. Martínez-Lope, and M. Hidalgo, *J. Solid State Chem.* **116**, 146 (1995).
- [22] J. Pérez, J. García, J. Blasco, and J. Stankiewicz, *Phys. Rev. Lett.* **80**, 2401 (1998).
- [23] P. Hansmann, X. Yang, A. Toschi, G. Khaliullin, O. K. Andersen, and K. Held, *Phys. Rev. Lett.* **103**, 016401 (2009).
- [24] H. Chen, D. P. Kumah, A. S. Disa, F. J. Walker, C. H. Ahn, and S. Ismail-Beigi, *Phys. Rev. Lett.* **110**, 186402 (2013).
- [25] A. S. Disa, D. P. Kumah, A. Malashevich, H. Chen, D. A. Arena, E. D. Specht, S. Ismail-Beigi, F. J. Walker, and C. H. Ahn, *Phys. Rev. Lett.* **114**, 026801 (2015).
- [26] G. Catalan, R. M. Bowman, and J. M. Gregg, *Phys. Rev. B* **62**, 7892 (2000).
- [27] N. Shukla, T. Joshi, S. Dasgupta, P. Borisov, D. Lederman, and S. Datta, *Appl. Phys. Lett.* **105**, 012108 (2014).
- [28] R. Mallik, E. V. Sampathkumaran, J. A. Alonso, and M. J. Martínez-Lope, *J. Phys.: Condens. Matter* **10**, 3969 (1998).
- [29] S. D. Ha, R. Jaramillo, D. M. Silevitch, F. Schoofs, K. Kerman, J. D. Baniecki, and S. Ramanathan, *Phys. Rev. B* **87**, 125150 (2013).
- [30] C. A. Jackson, J. Y. Zhang, C. R. Freeze, and S. Stemmer, *Nat. Commun.* **5**, 4258 (2014).
- [31] J. Liao, Y. Ou, X. Feng, S. Yang, C. Lin, W. Yang, K. Wu, K. He, X. Ma, Q.-K. Xue *et al.*, *Phys. Rev. Lett.* **114**, 216601 (2015).
- [32] See Supplemental Material at <http://link.aps.org/supplemental/10.1103/PhysRevB.94.235124> for DFT calculations of phonon modes in pristine SNO, other MR models in thin films and temperature effects of MR in oxygen deficient SNO.
- [33] R. Jaramillo, F. Schoofs, S. D. Ha, and S. Ramanathan, *J. Mater. Chem. C* **1**, 2455 (2013).
- [34] L. Zhang, H. J. Gardner, X. G. Chen, V. R. Singh, and X. Hong, *J. Phys.: Condens. Matter* **27**, 132201 (2015).
- [35] V. V. Poltavets, M. Greenblatt, G. H. Fecher, and C. Felser, *Phys. Rev. Lett.* **102**, 046405 (2009).
- [36] L. Zhang and Z.-J. Tang, *Phys. Rev. B* **70**, 174306 (2004).
- [37] A. Dakhel, *Cryst. Res. Technol.* **39**, 404 (2004).
- [38] M. Jenderka, J. Barzola-Quiquia, Z. Zhang, H. Frenzel, M. Grundmann, and M. Lorenz, *Phys. Rev. B* **88**, 045111 (2013).
- [39] N. Mott, *Philos. Mag.* **19**, 835 (1969).
- [40] N. Mott, *J. Non-Cryst. Solids* **1**, 1 (1968).
- [41] B. Pollak and M. Shklovskii, *Hopping Transport in Solids* (Elsevier/North Holland, Amsterdam, 1990).
- [42] B. I. Shklovskii and A. L. Efros, *Electronic Properties of Doped Semiconductors* (Springer-Verlag, Berlin, 1984).
- [43] C. G. Van de Walle, *Phys. Rev. Lett.* **85**, 1012 (2000).
- [44] W.-C. Hsu, C.-C. Chan, C.-H. Peng, and C.-C. Chang, *Thin Solid Films* **516**, 407 (2007).
- [45] C. Girardot, J. Kreisel, S. Pignard, N. Caillault, and F. Weiss, *Phys. Rev. B* **78**, 104101 (2008).
- [46] J. Ravichandran, C. R. Serrao, D. K. Efetov, D. Yi, Y. S. Oh, S.-W. Cheong, R. Ramesh, and P. Kim, *J. Phys.: Condens. Matter* **28**, 505304 (2016).
- [47] A. Frydman and Z. Ovadyahu, *Solid State Commun.* **94**, 745 (1995).
- [48] A. Vaknin, A. Frydman, Z. Ovadyahu, and M. Pollak, *Phys. Rev. B* **54**, 13604 (1996).
- [49] H. Fukuyama and K. Yoshida, *J. Phys. Soc. Jpn.* **46**, 102 (1979).
- [50] M. Eto, *Physica B (Amsterdam)* **194**, 1113 (1994).
- [51] S. D. Ha, G. H. Aydogdu, and S. Ramanathan, *J. Appl. Phys.* **110**, 094102 (2011).
- [52] H. Inoue, A. G. Swartz, N. J. Harmon, T. Tachikawa, Y. Hikita, M. E. Flatté, and H. Y. Hwang, *Phys. Rev. X* **5**, 041023 (2015).
- [53] J. García-Muñoz, J. Rodríguez-Carvajal, and P. Lacorre, *Europhys. Lett.* **20**, 241 (1992).
- [54] D. Kumar, K. P. Rajeev, J. A. Alonso, and M. J. Martínez-Lope, *Phys. Rev. B* **88**, 014410 (2013).
- [55] X. Chen, T. Hogan, D. Walkup, W. Zhou, M. Pokharel, M. Yao, W. Tian, T. Z. Ward, Y. Zhao, D. Parshall *et al.*, *Phys. Rev. B* **92**, 075125 (2015).
- [56] A. Nigam, R. Ray, T. Srinivasan, and A. Majumdar, *J. Appl. Phys.* **50**, 7361 (1979).
- [57] X. Wang, Q. Shao, A. Zhuravlyova, M. He, Y. Yi, R. Lortz, J. Wang, and A. Ruotolo, *Sci. Rep.* **5**, 9221 (2015).
- [58] M. Khalid and P. Esquinazi, *Phys. Rev. B* **85**, 134424 (2012).
- [59] I. Lorite, C. Zandalazini, P. Esquinazi, D. Spemann, S. Friedländer, A. Pöpl, T. Michalsky, M. Grundmann, J. Vogt, J. Meijer *et al.*, *J. Phys.: Condens. Matter* **27**, 256002 (2015).
- [60] B. Shklovskii, *Sov. Phys. Semicond.* **17**, 1311 (1983).
- [61] Z. Q. Liu, W. M. Lü, X. Wang, Z. Huang, A. Annadi, S. W. Zeng, T. Venkatesan, and Ariando, *Phys. Rev. B* **85**, 155114 (2012).
- [62] J. Hu, M. M. Parish, and T. F. Rosenbaum, *Phys. Rev. B* **75**, 214203 (2007).
- [63] A. Narayanan, M. D. Watson, S. F. Blake, N. Bruyant, L. Drigo, Y. L. Chen, D. Prabhakaran, B. Yan, C. Felser, T. Kong *et al.*, *Phys. Rev. Lett.* **114**, 117201 (2015).
- [64] M. A. Aamir, S. Goswami, M. Baenninger, V. Tripathi, M. Pepper, I. Farrer, D. A. Ritchie, and A. Ghosh, *Phys. Rev. B* **86**, 081203 (2012).
- [65] V. N. Prigodin, N. P. Raju, K. I. Pokhodnya, J. S. Miller, and A. J. Epstein, *Adv. Mater.* **14**, 1230 (2002).
- [66] N. P. Raju, V. N. Prigodin, K. I. Pokhodnya, J. S. Miller, and A. J. Epstein, *Synth. Met.* **160**, 307 (2010).
- [67] U. Bauer, L. Yao, A. J. Tan, P. Agrawal, S. Emori, H. L. Tuller, S. Van Dijken, and G. S. Beach, *Nat. Mater.* **14**, 174 (2015).